Journal of Solid State Chemistry 182 (2009) 3125–3130

Contents lists available at ScienceDirect

Journal of Solid State Chemistry

journal homepage: www.elsevier.com/locate/jssc

Novel building units with bimetallic rings in inorganic/organic hybrid chains and layers

Thushitha Mahenthirarajah, Yang Li, Philip Lightfoot *

EaStCHEM, School of Chemistry, University of St. Andrews, St. Andrews, Fife KY16 9ST, UK

ARTICLE INFO

Article history:
Received 2 July 2009
Received in revised form
25 August 2009
Accepted 30 August 2009
Available online 9 September 2009

ABSTRACT

Hydrothermal synthesis has produced three new compounds constructed from novel building units containing vanadium-oxide (or oxyfluoride) subunits linked together *via* covalently bound cationic copper complexes. Each new compound exhibits novel structural features: $[Cu(dipa)][VOF_4]$ (**1**) incorporates a corner-sharing octahedral vanadium(IV) oxyfluoride chain decorated by copper-(2,2′-dipyridyl amine) complexes which form *intra*-chain bridges. Within a similar reactant system $[Cu(dipa)]_2[V_6O_{17}]$ (**2**) is produced, the structure of which exhibits edge-sharing trigonal bipyramidal vanadium(V) 'ladder-like' double chains which are bridged into layers by tetrahedral pyrovanadate dimers together with the copper-(2,2′-dipyridyl amine) complexes. $[Cu(py)_4]_2[V_4O_{12}]$ (**3**), is a 2-D structure featuring exclusively tetrahedral vanadium(V) in four-membered ring building blocks, linked through octahedral copper-pyridine complexes to form two crystallographically different bimetallic layers.

1. Introduction

In recent years vanadium oxides and their derivatives have been much explored because of their potential applications in the field of electronics based on lithium-ion batteries [1] together with extended physical properties specifically magnetism, [2] non-linear optical ability (NLO), [3] luminescence [4] and ferroelectricity [5]. Further developments have been attained by defining vanadium-containing building blocks prepared by solvothermal synthesis. Zubieta and co-workers [6] introduced transition metals into the system, which contribute significantly by increasing the dimensionality and offering the potential for magnetic interactions, even though the vanadium still exhibits the +5 oxidation state. Recently Poeppelmeier and co-workers [7] have reported the crystal structure of $[Cu(py)_4VOF_4]$, a compound which exhibits both magnetic interactions as well as NLO properties. We have recently reported our exploration in vanadium oxyfluoride systems, which show a rich variety of oligomeric, [8,9] chain, [10] ladder-like [2] and 3-D network [11] structural elements. The diverse array of reaction variables can have a significant influence in these complex systems, for example the role of temperature in increasing dimensionality and decreasing vanadium oxidation states has been shown [12]. One way forward in studying such systems is to employ 'composition-space' diagrams, [13] as we have recently used in related Nb and Mo-containing systems [14].

In this paper, we expand on our recent exploratory work on extended structures of vanadium-based hybrids. A detailed composition-space diagram (Supplementary) has been used to isolate chain structure **1** and layer-structure **2**, whereby the V_2O_5/CuO /2,2′-dipyridylamine composition is varied in a systematic way while keeping low constant concentration of hydrofluoric acid (0.53 M) to produce phase stability fields which map out the chosen reaction products versus composition space. Fluoride is not incorporated into the products even though HF is present in the reaction medium of the layer structures **2** and **3**.

2. Experimental

2.1. Materials and methods

All chemicals were purchased from commercial sources and used without further purification. The CHN analyses were performed on a Carlo Erba EA1110. In addition, phase purity was confirmed by comparison of powder X-ray diffraction patterns simulated on the basis of the observed crystal structures to those measured experimentally by Rietveld refinement using the GSAS program [15].

2.2. General synthesis

$[Cu(C_{10}H_9N_3)]_2[VOF_4]_2$ (**1**), $[Cu(C_{10}H_9N_3)]_2[V_6O_{17}]$ (**2**) and $[Cu(C_5H_5N)_4]_2[V_4O_{12}]$ (**3**) were all synthesised hydrothermally in 27 ml Teflon-lined stainless steel autoclaves heated at 160 °C.

* Corresponding author.
E-mail address: pl@st-and.ac.uk (P. Lightfoot).

0022-4596/$ - see front matter © 2009 Elsevier Inc. All rights reserved.
doi:10.1016/j.jssc.2009.08.029

For **1**: 0.080 g (0.43×10^{-3} mol) of V_2O_5 was dissolved with 0.2 mL (1.2×10^{-2} mol) of 48% HF at room temperature. To the resultant solution was added 0.100 g (0.12×10^{-3} mol) of CuO and 0.150 g (0.88×10^{-3} mol) of 2,2-dipyridylamine ('dipa'=$C_{10}H_9N_3$). 4 mL water was added and stirred well until fully dissolved. The reaction vessel was sealed and heated to 160 °C for 2 days and then cooled to room temperature over an additional 24 h. The product was filtered off, washed with water and dried at 60 °C in air.

For **2**: Similar procedure as **1**, but using 0.200 g V_2O_5, 0.100 g CuO, 0.2 mL 48% HF, 0.050 g dipa and 10 mL water.

For **3**: Similar procedure as **1**, but using 0.200 g V_2O_5, 0.100 g CuO, 0.5 mL 48% HF, no dipa, 1.5 mL (4.8×10^{-2} mol) methylamine, 0.5 mL water and 5 mL (6.3×10^{-2} mol) pyridine. Reaction time in this case was 24 h.

In each case, phase purity was confirmed by elemental analysis and direct analysis for F^- using a fluoride-ion selective electrode [16], together with comparison of observed and simulated powder X-ray diffraction patterns (Supplementary). Elemental and crystallographic analyses are in good agreement with the structural formula $[Cu(C_{10}H_9N_3)]_2[VOF_4]_2$ (**1**) Calcd: C, 31.80%; H, 2.40%; N, 11.13%; F, 20.12%, measured: C, 31.61%; H, 2.27%; N, 10.89%; F, 19.78%; for $[Cu(C_{10}H_9N_3)]_2[V_6O_{17}]$ (**2**): Calcd: C, 22.94%; H, 1.73%; N, 8.03%, measured: C, 22.68%; H, 1.63%; N, 7.91%. Blue crystals of $[Cu(C_5H_5N)_4]_2[V_4O_{12}]$ (**3**) together with an uncharacterised powder phase were recovered by vacuum filtration; **3** decomposes in air at room temperature after a few days.

2.3. X-ray crystallography

Single-crystal X-ray diffraction data were collected with a Rigaku Mercury CCD with silicon monochromated Mo $K\alpha$. All of the datasets were corrected for absorption via multiscan methods. The structure were solved by direct methods and refined by full-matrix least-squares techniques using the SHELXS, SHELXL [17] and WinGX [18] packages. The final refinement includes anisotropic refinement for all non-hydrogen atoms, except in the case of **3**, where disorder was modeled around the vanadate groups of V(1), V(5) and V(6), such that these exist in two orientations with O atoms refined isotropically. All hydrogen atoms were located and refined using a riding model with isotropic displacement parameters. Crystallographic details are given in Table 1 and selected connectivity data including bond valence sum [19] (BVS) for metal centres in Table 2 The high *R*-factors for **1** can be explained by the presence of a twin, which nevertheless does not significantly affect the validity of the final model. The high *R*-factors for **3** are in part due to the presence of considerable disorder around the vanadate groups. Again, we believe the overall features of the structure are valid.

Powder X-ray diffraction data were collected on a Stoe STADI/P diffractometer-transmitting Cu$K\alpha$1 radiation at 1.5406 Å, via a curved germanium monochromator with a 2θ range from 5° to 70°. The data were collected overnight in order to obtain reliable Rietveld refinements based on the single-crystal models (i.e. using fixed atomic co-ordinates) to further confirm phase purity for magnetic measurements.

2.4. Magnetic measurements

Magnetic susceptibility data for **1** were measured on a Quantum Design MPMS SQUID. Data were recorded in 5000 Oe field while warming the sample from 2 to 300 K in 4 K steps following consecutive zero-field cooling (ZFC) and field-cooling (FC) cycles. The data were normalized to the molar quantity of the sample and any diamagnetic contributions were deducted from the total magnetic contribution before data fitting.

2.5. Results and discussion

In the low constant concentration of hydrofluoric acid (0.53 M), the crystallisations in the 2,2′-dipyridylamine system of **1**, **2** and $[Cu_2F_2(C_{10}H_{10}N_3)_2][V_2O_7]$[10] occur at relatively low mole percentage of V_2O_5 in comparison to CuO and 2,2′-dipyridylamine. At higher concentration of hydrofluoric acid (1.05 M) all products were green-coloured solutions with no solid product. At very low concentration of hydrofluoric acid (0.26 M), the metal oxides did not dissolve completely and formed poorly crystalline and charactersied powder. Changing the ratio of CuO to V_2O_5 resulted in three different phases. However, the reactant ratios do not directly relate to the crystal structure compositions. Changing the ratio of hydrofluoric acid and water content, while keeping other reactants and conditions as constant, was also carried out, but only at particular low concentration, yielding **2**.

The crystal structure of **1** reveals an infinite 1-D chain running along the *a*-axis, as shown in Fig. 2. The building unit contains two crystallographically different square-pyramidal copper centres

Table 1
Crystallographic data for structures **1**, **2** and **3**.

Compound	**1**	**2**	**3**
Formula	$[Cu(C_{10}H_9\ N_3)]_2[VOF_4]_2$	$[Cu(C_{10}H_9N_3)]_2[V_6O_{17}]$	$[Cu(C_5H_5N)_4]_2[V_4O_{12}]$
Formula weight	755.38	1047.14	1155.66
Crystal system	Triclinic	Triclinic	Monoclinic
Space group	*P*-1	*P*-1	$P2_1/c$
a(Å)	7.366 (3)	7.331 (1)	23.757 (6)
b(Å)	9.445 (3)	10.123 (1)	16.688 (4)
c(Å)	16.515 (4)	10.578 (1)	17.021 (4)
α	91.937 (7)	95.986 (4)	90
β	90.571 (6)	110.160 (4)	80.727 (6)
γ	92.767 (7)	92.605 (3)	90
Volume (Å^3)	1146.9 (6)	730.11 (16)	6660 (3)
Z	2	1	6
Total/unique	6076/3626	5153/2758	42,024/12,032
Ind. reflns $>2\sigma(I)$	2950	2423	5623
T (°C)	−180	−180	−180
λ (Å)	0.7107	0.7107	0.7107
ρ_{calcd} (g/cm^3)	2.19	2.382	1.729
$R1[I>2\sigma(I)]$	0.112	0.038	0.112
w$R2[I>2\sigma(I)]$	0.286	0.101	0.273

Table 2
Selected bond lengths and BVS for **1**, **2** and **3**.

1	2	3[a]
V1–O1 1.600 (10)	V1–O1 1.623 (3)	V1–O1 1.685 (12)
V1–F1 1.975 (8)	V1–O2 1.963 (3)	V1–O2 1.603 (9)
V1–F2 2.079 (9)	V1–O3 1.969 (3)	V1–O3 1.82 (2)
V1–F3 1.981 (8)	V1–O3′ 1.947 (3)	V1–O4 1.816 (15)
V1–F5 1.969 (8)	V1–O4 1.662 (3)	V2–O4 1.897 (16)
V1–F8 1.926 (8)	V2–O2 1.874 (3)	V2–O5 1.613 (7)
V2–O2 1.592 (10)	V2–O2′1.976 (3)	V2–O6 1.659 (8)
V2–F3 1.962 (8)	V2–O3 1.895 (3)	V2–O9 1.799 (7)
V2–F4 1.895 (7)	V2–O5 1.604 (3)	V3–O7 1.685 (7)
V2–F5 2.009 (8)	V2–O6 1.779 (3)	V3–O8 1.610 (7)
V2–F6 2.097 (9)	V3–O6 1.822 (3)	V3–O9 1.799 (7)
V2–F7 1.994 (8)	V3–O7 1.788 (1)	V3–O10 1.799 (7)
Cu1–F1 1.947 (9)	V3–8 1.621 (3)	V4–O3 1.769 (11)
Cu1–F2 1.945 (7)	V3–O9 1.666 (3)	V4–O10 1.802 (7)
Cu1–F4 2.139 (8)	Cu1–O4 1.968 (3)	V4–O11 1.621 (7)
Cu1–N1 1.945 (13)	Cu1–O8 2.259 (4)	V4–O12 1.607 (8)
Cu1–N2 1.967 (10)	Cu1–O9 1.931 (3)	V5–O13 1.837 (14)
Cu2–F6 1.908 (7)	Cu1–N1 1.975 (4)	V5–O14 1.985 (14)
Cu2–F7 1.940 (8)	Cu1–N2 1.982 (4)	V5–O15 1.789 (16)
Cu2–F8 2.286 (8)	∑(V1) 5.06	V5–O18 1.784 (15)
Cu2–N4 1.971 (11)	∑(V2) 5.01	V6–O13 1.813 (12)
Cu2–N5 1.967 (13)	∑(V1) 5.08	V6–O16 1.794 (9)
∑(V1) 3.80	∑(Cu1) 2.25	V6–O17 1.661 (14)
∑(V2) 3.82		V6–O18 1.818 (14)
∑(Cu1) 2.15		Cu1–O2 2.403 (8)
∑(Cu2) 2.08		Cu1–O12 2.326 (8)
		Cu1–N1 2.040 (11)
		Cu1–N2 2.016 (12)
		Cu1–N3 2.028 (10)
		Cu1–N4 2.035 (12)
		Cu2–O6 2.239 (8)
		Cu2–O7 2.401 (6)
		Cu2–N5 2.016 (8)
		Cu2–N6 2.031 (8)
		Cu2–N7 2.029 (8)
		Cu2–N8 2.069 (8)
		Cu3–O15 2.308 (12)
		Cu3–O16 2.264 (7)
		Cu3–N9 2.047 (7)
		Cu3–N10 2.043 (9)
		Cu3–N11 2.039 (8)
		Cu3–N12 2.054 (8)

[a] For **3** only one orientation of the disordered vanadate groups is given.

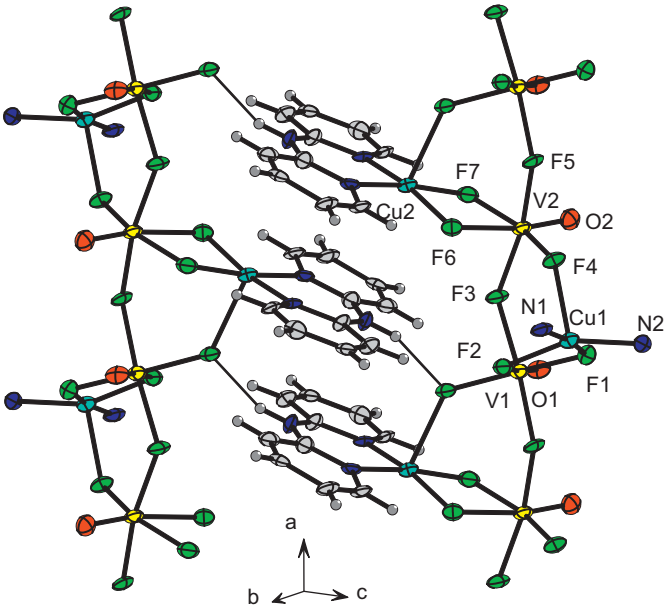

Fig. 1. Building elements and *inter*-chain hydrogen bonding interactions in **1**. Ellipsoids at 50% probability.

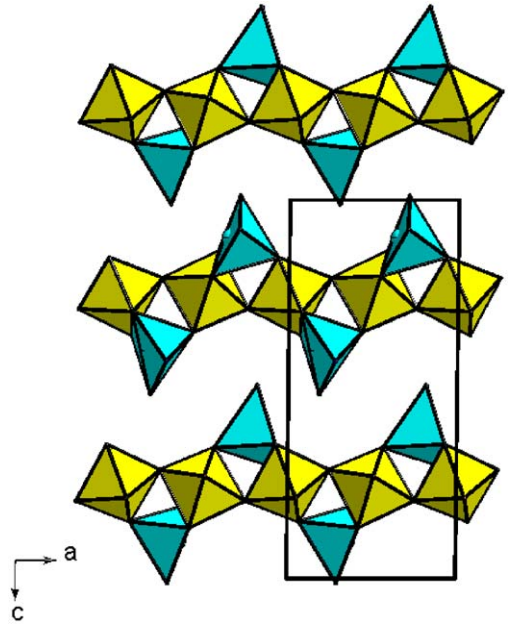

Fig. 2. Polyhedral representation of the inorganic sublattice of **1**. Cu-centred polyhedra lighter (yellow on-line) and V-centred polyhedra darker (blue on-line).

(Addison τ factors [20], which relate to the degree of square-pyramidal (τ=0)/trigonal-bipyramidal (τ=1) nature are 0.24 and 0.10 for Cu(1) and Cu(2), respectively) present in the +2 oxidation state together with two distinct octahedral vanadium centres in the +4 oxidation state, as confirmed by BVS analysis (Table 2). Each copper centre forms a three-membered bimetallic ring with two distinct vanadium centres linking through fluoride ligands. Each vanadium octahedron shares its edge with copper as well as sharing a corner with crystallographically different vanadium and copper (Fig. 1). The bulky bidentate ligand favours the copper complexes linking to a vanadium centre in a *trans* manner. The anion unit $[VOF_5]^{3-}$ adopts a distorted octahedral environment consistent with the presence of a short V=O bond, *cis* and *trans* positions are occupied by fluoride ligands coordinating to the copper complex. Further, these nucleophilic fluoride ligands accept hydrogen bonds from dipyridylamines of neighbouring chains thus forming a supramolecular 3-D network (N-H…F 1.92–2.11 Å; N…F 2.74–2.96 Å) (Fig. 1). The oxide ligands of the anion motifs neither coordinate to the copper centre nor accept a hydrogen bond. The vanadium oxyfluoride forms a continuous chain and the copper complex acts as 'decoration' to the chain rather than being directly involved in chain formation itself (Fig. 2).

Above 50 K, the magnetic susceptibility of **1** obeys a Curie–Weiss law, as shown in Fig. 3. A fit to the inverse susceptibility versus T plot (for $T > 50$ K) reveals a small negative Weiss constant ($\theta = -4.3$ K), which corresponds to antiferromagnetic ordering. However, the $\chi_\rho T$ versus T plot reveals a more complex behaviour, with an upturn around 30 K, suggestive of ferrimagnetism. This probably arises from competing interactions and ensuing frustration in the spin-1/2 "V_2Cu" three-membered ring units. The ratio of the 'ordering' temperature ($\sim$30 K) and the value of θ indicates the presence of weak geometric frustration according to Ramirez [21]. The value of μ_{eff}=3.43 BM obtained from the

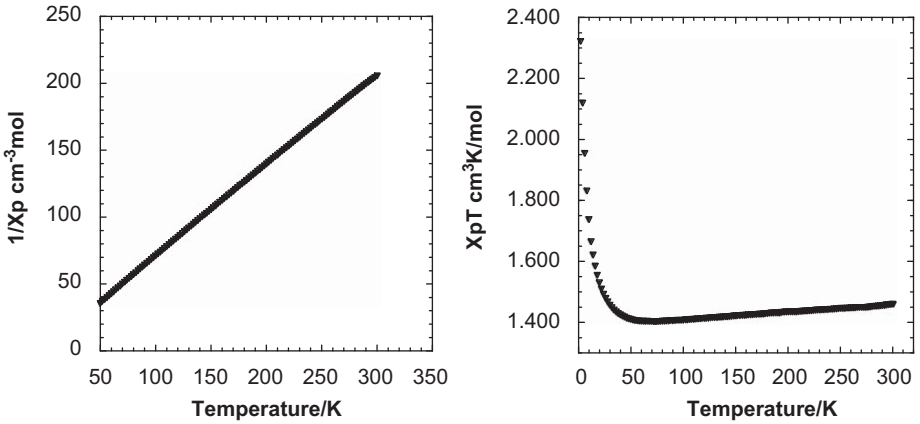

Fig. 3. $\chi_\rho{}^{-1}$ vs. T showing Curie-Weiss behaviour above 50 K (left) and $\chi_\rho T$ vs. T (right) for **1**.

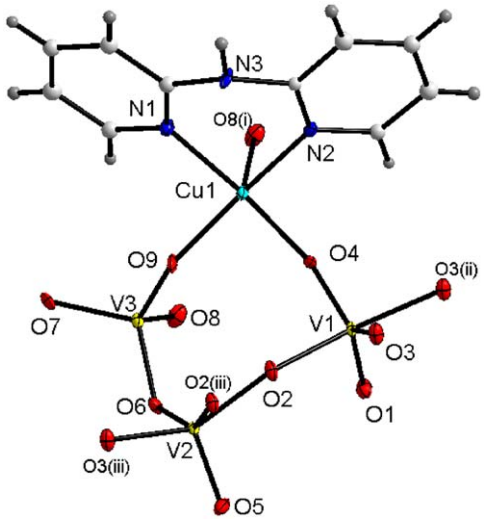

Fig. 4. The building unit in **2**. Symmetry operators (i) $1-x,-y,-z$;(ii) $2-x,-y,1-z$, (iii) $1-x,-y,1-z$.

Curie–Weiss plot is consistent with the ideal system of four non-interacting isolated spin-1/2 centres per formula unit (μ_{eff}=3.46 BM), also confirming the BVS analysis of V^{4+} and Cu^{2+}. The saturation value C in the $\chi_\rho T$ versus T plot is 1.49 $cm^3\,mol^{-1}\,K$ which is exactly the ideal value for the proposed model.

$[Cu(C_{10}H_9N_3)]_2[V_6O_{17}]$ (**2**) and $[Cu(C_5H_5N)_4]_2[V_4O_{12}]$ (**3**) exhibit novel 2-D structures. Fluoride is not incorporated into the products even though HF is present in the reaction medium.

The crystal structure of **2** illustrates some interesting features of hybrid inorganic/organic materials. The asymmetric unit (Fig. 4) contains a four-membered metal ring $[CuV_3]$ linked through oxide ligands, which contains two '2+3' square pyramidal (τ=0.36 and 0.08 for V(1), V(2), respectively) and one tetrahedral vanadium, all in the +5 oxidation state and a single Cu(II) in a square pyramidal (τ=0.23), '4+1', geometry (Table 2). The vanadate polyhedra share their edges forming an infinite double chain like a 'ladder' with a formula $[V_2O_5]_n$ parallel to the *a*-axis (Fig. 5). A similar type of double chain of edge-sharing polyhedra has been observed [22] in β-$NaVO_3$. The V–O distances forming the 'rungs' within these V_2O_5 ladders are comparable in both structures, for β-$NaVO_3$, 1.979(16) Å and for **2**; 1.969(3) Å and 1.976(3) Å. In the terminology of Zavalij and Whittingham [23], these chains may be described as [UD] type (i.e. 'up-down' alternating edge-shared square pyramids). Such chains are joined directly together to form layers in V_2O_5 itself in the present compound a novel means of joining these [UD] chains is encountered. The tetrahedral vanadium forms a V_2O_7 dimer which engages exclusively in corner-sharing interactions. Two oxygen sites of each tetrahedron contribute to bridge copper and the other site connecting the every third particular polyhedron of the ladder. The V_2O_7 groups interconnect neighbouring double chains into infinite vanadium-oxide layers parallel to the *ac* plane. The coordination environment of copper contains three bridging oxide ligands of tetrahedral vanadiums and a bidentate 2,2′-dipyridylamine ligand. The copper complex and tetrahedral vanadium form a bimetallic ring, $[Cu_2V_2]$, which is alternately linked to either side of the V_2O_5 double chain, forming a 2-D layer (Fig. 5). Effectively the copper complex could be regarded as an additional molecular moiety independent of the vanadium-oxide substructure, which then coordinates to the V–O sublattice. This framework contains different sizes of bimetallic Cu–V rings such as $[CuV_3]$, $[Cu_2V_2]$, $[CuV_4]$ and $[CuV_6]$. The 2,2′-dipyridylamine moieties of the copper complex are situated in between the layers, forming hydrogen bonds with oxygens coordinated to the vanadium atoms. Overall the 3-D supramolecular network is dominated by inter-layer hydrogen bonding interactions with distances of N3-H3A…O1 2.04 Å; N3…O1 2.89 Å (Fig. 6).

Compound **3** exhibits a 2-D structure featuring exclusively tetrahedral vanadium as a building block. We note that there is considerable disorder around some of the tetrahedral vanadate groups, such that they are effectively adopting two orientations 'inverted' relative to each other. The tetrahedra form four-membered ring motifs, linked through octahedral copper complexes to produce a bimetallic framework, rather than being simple-chain substructures. The asymmetric unit (Fig. 7) is complex and contains six crystallographically different vanadium sites all adopting tetrahedral geometry with a coordination environment consisting of three bridging oxide ligands and a terminal vanadyl bond and copper present in the +2 oxidation state in a '4+2' octahedral environment (Table 2). The layered assembly is constructed from four corner-sharing tetrahedra forming a four-membered vanadate ring, $[V_4]$, linked through octahedra, $[CuO_2N_4]$, in the *bc* plane. There are two crystallographically different layers with the same composition stacked alternately in a 2:1 ratio parallel to the *a*-axis (Fig. 9). Each layer contains two different sizes of open rings; a vanadate ring, $[V_4]$, and a 12-membered copper/vanadium bimetallic ring, $[Cu_4V_8]$. The pyridyl ligands coordinated to copper project into

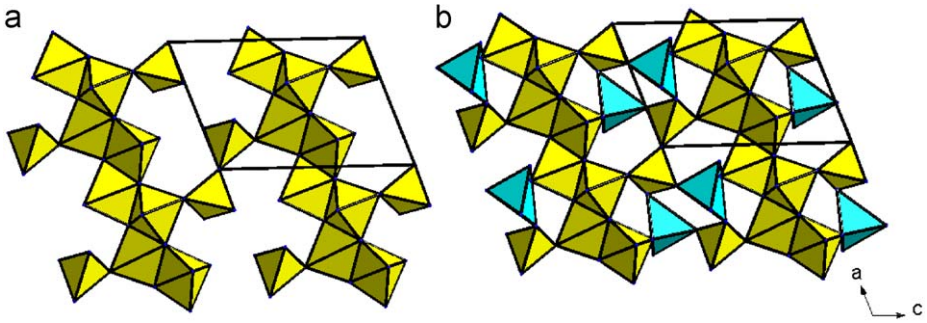

Fig. 5. (a) Double 'ladder'-like chain of $[V_2O_5]_n$ linked by bridging V_2O_7 groups, producing a continuous V–O layer into which the copper–amine complex is coordinated. (b) Resulting $[Cu_2V_2]$ rings, forming a 2-D layer in **2**, carbon and hydrogen atoms have been omitted for clarity.

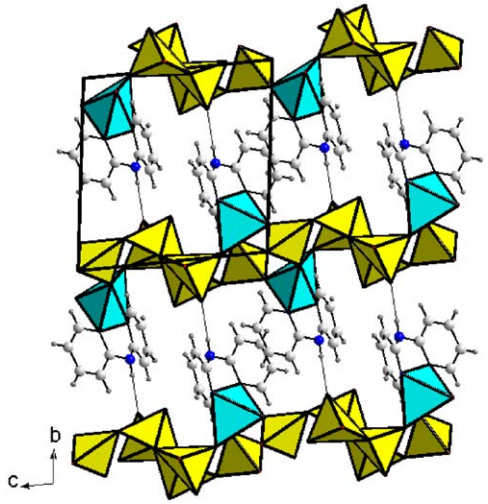

Fig. 6. Packing of **2** showing *inter*-layer hydrogen bonding interactions of the supramolecular network.

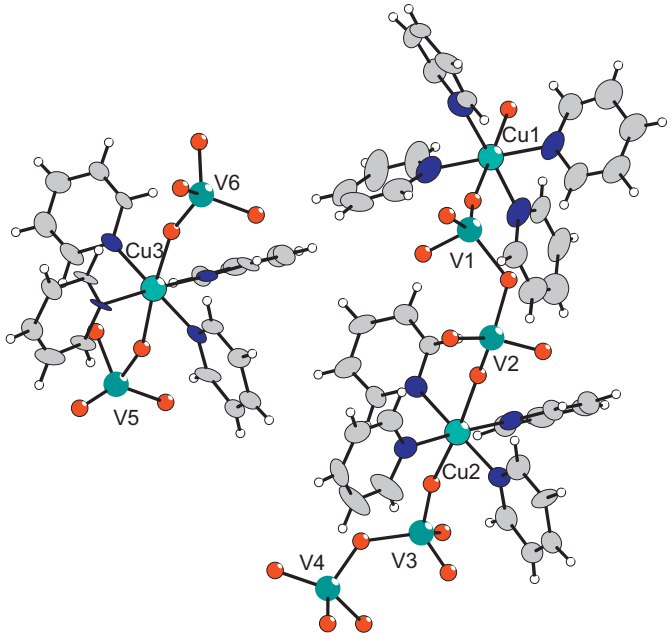

Fig. 7. The asymmetric unit in **3**. Symmetry operators (i) $x, 3/2-y, -1/2+z$; (ii) $x, 1+y, z$; (iii) $x, 3/2-y, 1/2+z$ and (iv) $-1-x, -1/2+y, 3/2-z$. Note that only one orientation of the disordered (isotropic) vanadate groups around V(1), V(5) and V(6) is shown.

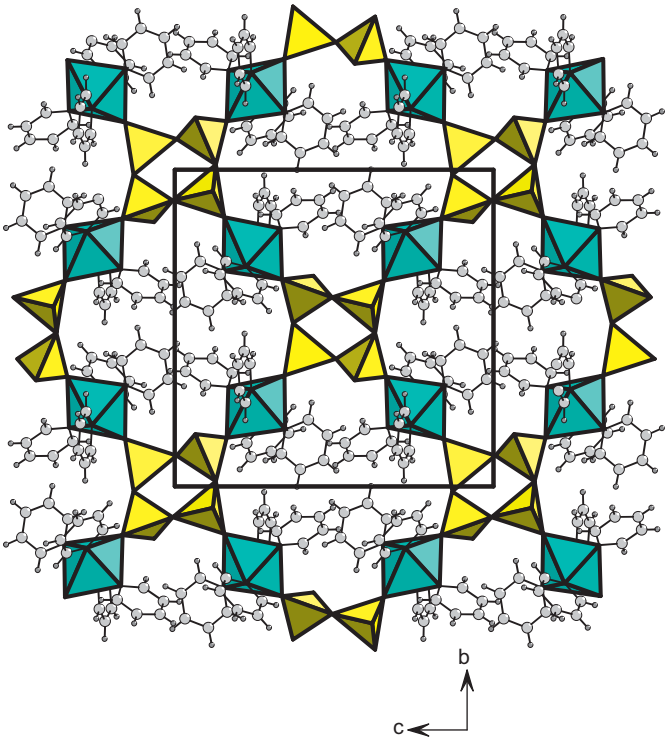

Fig. 8. A single inorganic layer in **3**, also showing pyridyl ligands coordinated to copper projecting into the 12-membered bimetallic ring. Only one orientation of the disordered vanadate groups is shown.

the 12-membered bimetallic ring as well as in between the layer cavity, as shown in Figs. 8 and 9.

3. Conclusions

Using solvothermal synthesis in HF-containing media three new compounds have been isolated, which display chain and layer structures with novel building units containing bimetallic ring motifs. Our systematic synthetic studies were carried out based on 'composition-space' diagram by varying the reaction composition to map out the crystallization field of the reactant system of **1** and **2**. However, in the case of **2** and **3**, fluoride is not incorporated into the products even though HF is present in the reaction medium. So far, based on the reactant composition as the systematic variable in the composition-space diagram of the

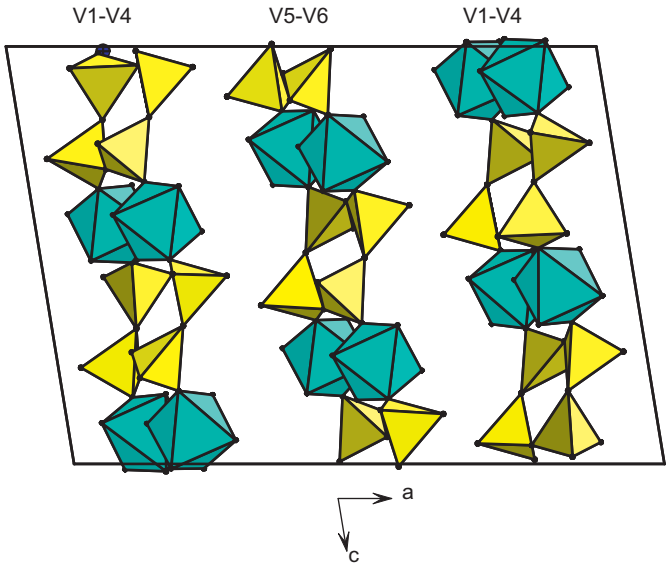

Fig. 9. The two different layers in **3**, alternately stacked together parallel to the *a*-axis; carbon and hydrogen atoms have been omitted for clarity. Only one orientation of the disordered vanadate groups is shown.

V_2O_5/CuO /2,2'-dipyridylamine system, we have only found crystallizations field with 1-D and 2-D structures, and the reactant ratios do not directly relate to the crystal structure composition. There are, however, still vast solvothermal reaction domains remaining to be explored such as pH, temperature, etc. and it may be anticipated that further novel structural features will be discovered in similar systems, in due course leading to novel physical properties.

Supplementary information

Crystallographic data in CIF format. Crystallographic data have also been deposited with CCDC (Deposition numbers 743910–743912).

Acknowledgements

We thank EaStCHEM for funding and Dr. R.J. Goff and Prof. A.M.Z. Slawin for helpful discussions.

Appendix A. Supplementary Materials

The online version of this article contains additional supplementary data. Please visit doi:10.1016/j.jssc.2009.08.029.

Appendix B. Supplementary Materials

References

[1] J. Howing, Acta Crystallogr. B25 (2003) 747.
[2] D.W. Aldous, R.J. Goff, J.P. Attfield, N.F. Stephens, P. Lightfoot, Inorg. Chem. 46 (2007) 461277.
[3] M.E. Welk, A.J. Norquist, C.L. Stern, K.R. Poeppelmeier, Cryst. Growth Des. 7 (2007) 956.
[4] L. Wang, Y. Li, Chem. Mater. 19 (2007) 727.
[5] J.J. Ravez, J. Phys. III 7 (6) (1997) 1129.
[6] P.J. Hagrman, C. Bridges, J.E. Greedan, J.J. Zubieta, J. Chem. Soc. Dalton Trans. (1999) 2901.
[7] M.E. Welk, C.L. Stern, K.R. Poeppelmeier, A. Norquist, J. Cryst. Growth. Des. 7 (2007) 956.
[8] N.F. Stephens, M. Buck, P. Lightfoot, J. Mater. Chem. 15 (2005) 4298.
[9] D.W. Aldous, N.F. Stephens, P. Lightfoot, Dalton Trans. (2007) 2271.
[10] T. Mahenthirarajah, Y. Li, P. Lightfoot, Inorg. Chem. 47 (2008) 9097.
[11] T. Mahenthirarajah, P. Lightfoot, Chem. Commun. (2008) 1401.
[12] D.W. Aldous, N.F. Stephens, P. Lightfoot, Dalton Trans. (2007) 4207.
[13] A.J. Norquist, K.R. Heier, C.L. Stern, K.R. Poeppelmeier, Inorg. Chem. 37 (1998) 6495.
[14] T. Mahenthirarajah, Y. Li., P. Lightfoot, Dalton Trans. (2009) 3280.
[15] A.C. Larson, R.B. Von Dreele, General Structure Analysis System (GSAS), Los Alamos National Laboratory Report LAUR, 2004, pp.86–748.
[16] H. Casellas, A. Pevec, B. Kozlevcar, P. Gamez, J. Reedijk, Polyhedron 24 (2005) 1549.
[17] G.M. Sheldrick, Acta Crystallogr. A64 (2008) 112.
[18] L.J. Farrugia, WinGX, J. Appl. Crystallogr. 32 (1999) 837.
[19] I.D. Brown, J. Solid State Chem. 82 (1989) 122.
[20] A.W. Addison, T.N. Rao, J. Reedijk, G.C. Verschoor, J. Chem. Soc. Dalton Trans. (1984) 1349.
[21] A.P. Ramirez, Annu. Rev. Mater. Sci. 24 (1994) 453.
[22] K. Kato, E. Takayama, Acta Crystallogr. B40 (1984) 102.
[23] P. Zavalij, M.S. Whittingham, Acta Crystallogr. B55 (1999) 627.